Progress Towards High Performance Plasmas in the National Spherical Torus Experiment (NSTX)

S.M. Kaye 1), M.G. Bell 1), R.E. Bell 1), S. Bernabei 1), J. Bialek 2), T. Biewer 1), W. Blanchard 1), J. Boedo 3), C. Bush 4), M.D. Carter 4), W. Choe 5), N. Crocker 6), D.S. Darrow 1), W. Davis 1), L. Delgado-Aparicio 7), S. Diem 1), J. Ferron 8), A. Field 9), J. Foley 1), E.D. Fredrickson 1), D.A. Gates 1), T. Gibney 1), R. Harvey 10), R.E. Hatcher 1), W. Heidbrink 11), K. Hill 1), J.C. Hosea 1), T.R. Jarboe 12), D.W. Johnson 1), R. Kaita 1), C. Kessel 1), S. Kubota 6), H.W. Kugel 1), J. Lawson 1), B.P. LeBlanc 1), K.C. Lee 13), F. Levinton 14), R. Maingi 4), J. Manickam 1), R. Maqueda 14), R. Marsala 1), D. Mastrovito 1), T.K. Mau 3), S.S. Medley 1), J. Menard 1), H. Meyer 9), D.R. Mikkelsen 1), D. Mueller 1), T. Munsat 15), B.A. Nelson 12), C. Neumeyer 1), N. Nishino 16), M. Ono 1), H. Park 1), W. Park 1), S. Paul 1), T. Peebles 6), M. Peng 4), C. Phillips 1), A. Pigarov 3), R. Pinsker 8), A. Ram 17), S. Ramakrishnan 1), R. Raman 12), D. Rasmussen 4), M. Redi 1), M. Rensink 18), G. Rewoldt 1), J. Robinson 1), P. Roney 1), L. Roquemore 1), E. Ruskov 11), P. Ryan 4), S.A. Sabbagh 2), H. Schneider 1), C. Skinner 1), A. Sontag 2), V. Soukhanovskii 18), T. Stevenson 1), D. Stotler 1), B. Stratton 1), D. Stutman 7), D. Swain 4), E. Synakowski 1), Y. Takase 19), G. Taylor 1), K. Tritz 7), A. von Halle 1), M. Wade 4), R. White 1), J. Wilgen 4), M. Williams 1), J.R. Wilson 1), W. Zhu 2), S.J. Zweben 1), R. Akers 9), P. Beiersdorfer 18), R. Betti 20), T. Bigelow 4), M. Bitter 1), P. Bonoli 17), C. Bourdelle 21), C.S. Chang 22), J. Chrzanowski 1), C. Domier 13), L. Dudek 1), P.C. Efthimion 1), M. Finkenthal 7), E. Fredd 1), G.Y. Fu 1), A. Glasser 23), R.J. Goldston 1), N.L. Greenough 1), L.R. Grisham 1), N. Gorelenkov 1), L. Guazzotto 20), R.J. Hawryluk 1), J. Hogan 4), W. Houlberg 4), F. Jaeger 4), M. Kalish 1), S. Krasheninnikov 3), J. Lawrence 24), D. Liu 11), N.C. Luhmann 13), E. Mazzucato 1), G. Oliaro 1), D. Pacella 25), R. Parsells 1), M. Schaffer 8), I. Semenov 26), K.C. Shaing 27), M.A. Shapiro 17), P. Sichta 1), D. Smith 1), X. Tang 23), R. Vero 7), W. Wampler 28)

1) Princeton Plasma Physics Laboratory, Princeton University, Princeton, NJ, USA
2) Dept. of Applied Physics, Columbia University, NYC, NY, USA
3) University of California, San Diego, CA, USA
4) Oak Ridge National Laboratory, Oak Ridge, TN, USA
5) Korea Advanced Institute of Science and Technology, Taejon, Republic of Korea
6) University of California, Los Angeles, CA, USA
7) Johns Hopkins University, Baltimore, MD, USA
8) General Atomics, San Diego, CA, USA
9) Euratom-UKAEA Fusion Association, Abingdon, Oxfordshire, UK
10) Compx, Del Mar, CA, USA
11) University of California, Irvine, USA
12) University of Washington, Seattle, WA, USA
13) University of California, Davis, CA, USA
14) Nova Photonics, Princeton, NJ, USA
15) University of Colorado, Boulder, CO, USA
16) Hiroshima University, Hiroshima, Japan
17) Massachusetts Institute of Technology, Cambridge, MA, USA
18) Lawrence Livermore National Laboratory, Livermore, CA, USA
19) Tokyo University, Tokyo, Japan
20) University of Rochester, Rochester, NY, USA
21) CEA Cadarache, France

22) New York University, NYC, NY, USA
23) Los Alamos National Laboratory, Los Alamos, NM, USA
24) Princeton Scientific Instruments, Princeton, NJ, USA
25) ENEA, Frascati, Italy
26) Kurchatov Institute, Russia
27) University of Wisconsin, Madison, WI, USA
28) Sandia National Laboratory, Albuquerque, NM, USA

e-mail contact of main author: skaye@pppl.gov

Abstract. The major objective of the National Spherical Torus Experiment (NSTX) is to understand basic toroidal confinement physics at low aspect ratio and high β_T. Research over the past two years has taken advantage of improvements in plasma control, which led to routine operation at high elongation and high β_T (up to ~40%) lasting for many energy confinement times. The installation of an active error field correction coil pair has opened up operation at low density and has allowed for initial resonant error field amplification experiments. The determination of the confinement and transport properties of NSTX plasmas has benefited greatly from the implementation of higher spatial resolution kinetic diagnostics. The transport is highly dependent on details of both the flow and magnetic shear. The parametric variation of confinement is similar to that at conventional aspect ratio but with enhanced values and with a strong B_T dependence. Core turbulence was measured for the first time in an ST through correlation reflectometry, showing significant contributions from magnetic fluctuations. Non-inductive startup has been explored using PF-only and transient co-axial helicity injection techniques, resulting in up to 140 kA of toroidal current. Calculated bootstrap and beam-driven currents have sustained up to 60% of the flattop plasma current in NBI discharges. Studies of HHFW absorption have indicated parametric decay of the wave and associated edge thermal ion heating. Energetic particle modes, most notably TAE and fishbone-like modes, have indicated particle losses, and these instabilities may affect fast ion confinement on devices such as ITER. Finally, a variety of techniques has been developed for fueling and power and particle control.

1. Introduction

The National Spherical Torus Experiment (NSTX) [1-3] is a low aspect ratio torus whose goals are to advance the understanding of basic toroidal confinement physics using the leverage of high β_T ($=\langle p\rangle/(B_{T0}^2/2\mu_0)$) and low aspect ratio to help develop the physics basis for advancing the Spherical Torus (ST) concept [4,5]. To do this, an experimental database and a theoretical understanding must be developed in four areas: macroscopic plasma behavior, transport, waves and energetic particles, and plasma-boundary interfaces. NSTX goals in each area include:

1) *Macroscopic Plasma Behavior:* Attainment of wall stabilized plasmas with β_T~40% and β_N up to 9, compatible with non-inductive current startup and sustainment;
2) *Transport:* Routine access to long-pulse plasmas with confinement enhanced by at least 60% over L-mode values;
3) *Waves and Energetic Particles:* The ability to heat electrons selectively and drive current non-inductively using RF waves, and good confinement of energetic particles in the super-Alfvénic regime;
4) *Plasma Boundary Interface:* Density control and the ability to operate the compact ST configuration with low heat flux to the walls.

NSTX is both addressing these issues individually and is integrating the best conditions of each in order to develop steady-state, high performance plasmas. While the international ST program is widely based and varied [6-8], NSTX is uniquely positioned to address the high performance issues described above. This paper presents the highlights of NSTX research over the last two years. The device capabilities and diagnostics are described in Section 2 with emphasis on the new capabilities commissioned in 2003-2004. Progress towards the main goals in each physics area will be given in Section 3, and progress towards developing integrated high-performance scenarios will be described in Section 4.

2. Device description and capabilities

NSTX operates at low aspect ratio with R=0.85 m and a=0.67 m (R/a≈1.27). Over the past two years, NSTX has operated with plasma currents up to 1.4 MA, B_T up to 0.45 T and elongations up to 2.6 in both the Lower Single Null (LSN) or Double Null Diverted (DND) configurations. Deuterium neutral beam power of just over 7 MW at 100 keV and HHFW power of up to 6 MW at 30 MHz are sources of heating and non-inductive current drive. Plasma operation was primarily in deuterium; helium was sometimes used during HHFW operation. Close-fitting conducting plates provide passive stabilization of vertical motion and external MHD modes; the inner and outer halves of the vessel are isolated electrically for generating plasma current non-inductively through co-axial helicity injection (CHI).

Key facility upgrades over the past two years included a multi-barrel lithium pellet injector, a supersonic gas injector, a capacitor bank power supply for CHI experiments, and modifications to the HHFW antenna feedthroughs for increasing the power delivered to the plasma. The latency in the plasma control system was reduced, improving vertical control [9]. Continued development of real-time EFIT (rtEFIT [10]) led to its successful use in experiments that required fine boundary control. An extra set of PF coils was commissioned for use in non-solenoidal startup experiments, and a pair of ex-vessel control coils for error field compensation and control of Resistive Wall Modes (RWM) was installed and operated.

The past two years also saw improvements in the NSTX diagnostics. A new 51-channel Charge Exchange Recombination Spectroscopy (CHERS) diagnostic for measuring ion temperature, toroidal rotation velocity and carbon density profiles was installed. Additional new diagnostics included an Edge Rotation Diagnostic (ERD) to measure simultaneously the poloidal and toroidal rotation, temperature and density of both C^{2+} and He^{1+} ions at the plasma edge, magnetic sensors in the divertor region to aid equilibrium reconstruction, internal magnetic sensors for measuring the n=1 to 3 mode structures of external/RWM modes, and a high frequency RF probe. A scanning Neutral Particle Analyzer (NPA) was installed to measure the thermal and fast ion distribution functions, and a reflectometer system was upgraded to enable measurements of long-λ turbulence in the plasma core through correlation reflectometry. Edge fluctuations were measured with an upgraded reciprocating edge probe, a new fast camera for Gas Puff Imaging (GPI) measurements, a new divertor camera and edge channels in the FIR interferometer system (FIRETIP). Finally, an eight channel Motional Stark Effect diagnostic was installed and used to measure the plasma current profile.

3. Experimental Results

3.1. Macroscopic Plasma Behavior

Access to high β_T became more frequent, and for longer duration, due to a reduction in the time response of the plasma control system from 4 to 0.75 msec [9]. This improvement in the feedback control for vertical position in 2004, along with techniques to induce an early L-H transition, led to routine operation at higher elongation, κ, and triangularity, δ, and longer pulse lengths. This is characterized by plotting the effective magnetic pulse length, $\tau_{p,mag}$, as a function of κ in Fig. 1. $\tau_{p,mag}$ is defined as $(\int I_p\, dt)/I_{TF}$ for $I_p > 0.85 I_{p,max}$. I_{TF} is the total TF coil threading current. The weighting in $\tau_{p,mag}$ by the magnetic utilization factor, I_p/I_{TF}, normalizes

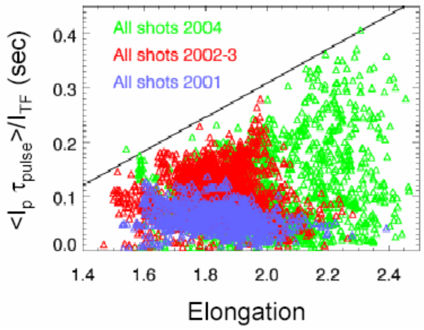

FIG. 1 Magnetic pulse length vs elongation, κ, for NSTX

out differences due to q, since $I_p/I_{TF} \propto 1/q_{cyl}$ for fixed ε (a/R). The elongation was calculated by the magnetics-based equilibrium reconstruction code EFIT, adapted for use on NSTX [11]. The control system improvement extended operations in elongation; κ-values exceeding 2.6 and δ up to 0.8 were obtained. A ~20% increase over the previous maximum elongation is seen.

The improved vertical control also led to a greater number of discharges at high values of normalized current, I_p/aB_T, and hence high values of β_T. Shown in Fig. 2a is a plot of plot of peak β_T as determined from EFIT for a subset of discharges shown in Fig. 1. The EFIT calculations were based on external magnetic measurements with the pressure profile shape constrained by the electron pressure as measured by the Thomson scattering diagnostic. The error bar is the EFIT random uncertainty in the value of β_T. Values of the normalized β, $\beta_N = \beta_T/(I_p/aB_T)$, up to 6.2 %·m·T/MA at the time of peak β_T were attained over the full range of I_p/aB_T. A maximum value of β_N= 6.8 %·m·T/MA has been achieved. The benefit of being able to achieve higher κ and thus higher I_p/aB_T is evidenced by significantly more high-β_T (>30%) shots during the 2004 experimental campaign than in previous years [12].

Longer duration periods of high β_T were achieved as well. Fig. 2b shows a time evolution of a 1 MA, high- β_T discharge. In this discharge, early neutral beam injection and a short pause in the plasma current ramp led to an early L-H transition [13]. The TF was ramped down at 0.34 s after an ELM-free period. During the ramp, the stored energy of the plasma plateaued at 250 kJ while β_T continued to increase. Also shown is the β_T evolution as computed by TRANSP, which is based on the measured kinetic profiles of the thermal ions and electrons and a Monte-Carlo calculation of the neutral beam ion component based on classical processes. The kinetic profiles as measured by the CHERS and Thomson Scattering diagnostics for the high-β_T shot at t=0.55 s are shown in Fig. 3, and they exhibit strong rotational shear and sharp gradients in T_i and T_e. The β_T values from the magnetic and kinetic calculations peak at 36 and 38% respectively (Fig. 2b). A significant result is that the EFIT β_T remained high (>30%) for approximately 0.08 s, which is about two energy confinement times. The earlier decrease in

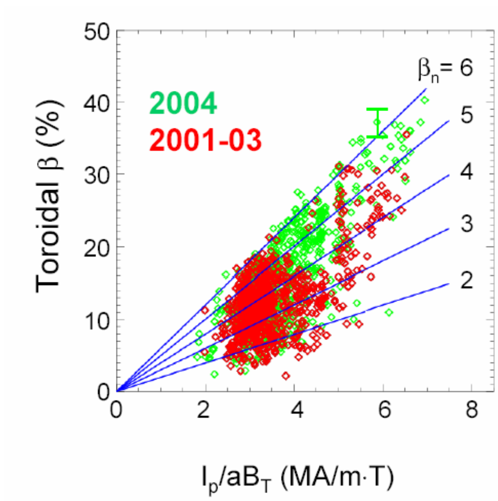

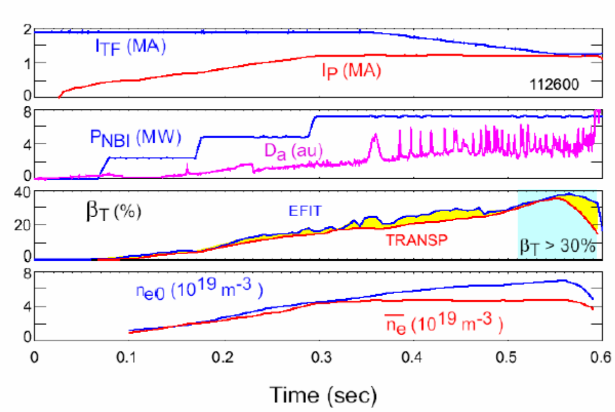

Fig. 2a β_T vs I_p/aB_T *2b Time evolution of high-β_T discharge*

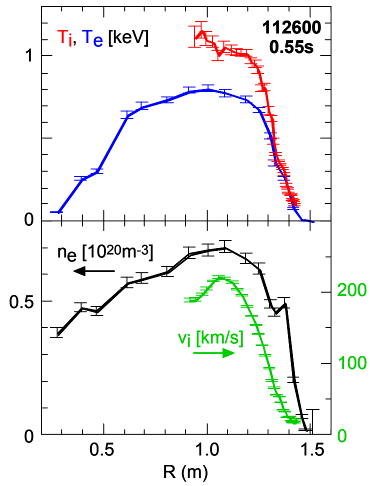

FIG. 3 CHERs profiles for high-β_T discharge.

in the TRANSP β_T is due to sparser time resolution of the kinetic profile measurements as compared to that of the magnetics. The edge density was controlled by the ELMs, as indicated by the density traces in the bottom panel of Fig. 2b. The β_T in this high-β_T discharge was limited by the growth of internal 1/1 MHD modes, modified by sheared rotation and/or diamagnetic effects [14].

The stabilization of performance limiting MHD modes was explored using the first of three pairs of error field (EF)/RWM control coils. The active control coil pair was used to eliminate low density locked modes which otherwise limit the potential for achieving high performance plasmas, as well as to understand the effect of the applied radial magnetic fields on modes at higher density and β_T. In the appropriate polarity with with 1 kA-turn, corresponding to an applied n= 1 B_{radial} ~10 G at the outer midplane, locked modes could be eliminated, with the locked mode density threshold reduced from 1.2 to $0.5\text{-}0.6{\cdot}10^{19}$ m^{-3}.

The elimination of the low density locked mode by use of this coil expands the NSTX operating space, aids HHFW operation at low density and allows for the study of possible performance limiting modes at higher density and β_T. One such mode is the RWM, which can be excited by the applied B_{radial}. Fig. 4 shows an example of resonant field error amplification (RFA) in which the excited mode is manifest as an n=1 locked mode as the plasma continued to rotate. The RFA gain (locked mode amplitude per current in the active coil) increased with β_N above the no-wall limit (>4.9) as calculated by DCON [15]. Future work will focus on using the EF/RWM coil to to suppress the low density locked modes and the RFA simultaneously [16].

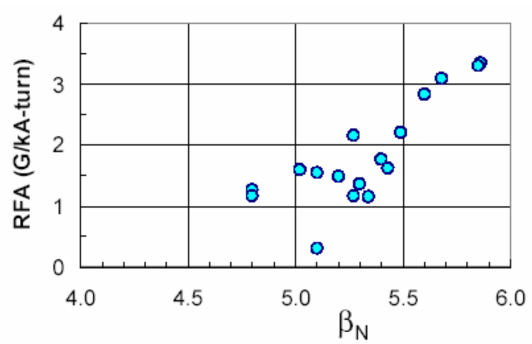

FIG. 4 RFA gain vs β_N

Non-inductive operation will be a critical issue for future STs because of space and neutron loading limitations. Several techniques of non-solenoidal plasma startup are being explored on NSTX. In initial experiments in one technique, plasmas were pre-ionized using HHFW and ECH on the outside of the vessel near the RF antenna. PF coil currents were initially adjusted to establish a high quality field null ($B_\phi E_\phi/B_\theta$>0.1 kV/m) over a substantial portion of the plasma, and then they were ramped to produce a toroidal loop voltage of 5 to 15 Volts near the antenna. Currents up to 20 kA were produced, but the plasmas terminated on the center stack. The challenge for this technique is to control the radial position of the nascent plasma to confine it to the region where the loop voltage is high, and thus achieve higher current.

Another technique that was tested is transient CHI [7], in which a pulse of voltage lasting for only a few ms was applied between the inner and outer vessel segments, causing plasma breakdown and generating a toroidal current which was propelled into the main chamber. The transient CHI technique has the benefit of reduced power to the walls, since the CHI is on for only a short time. An example of a CHI discharge in NSTX is shown in Fig. 5. A voltage of 1

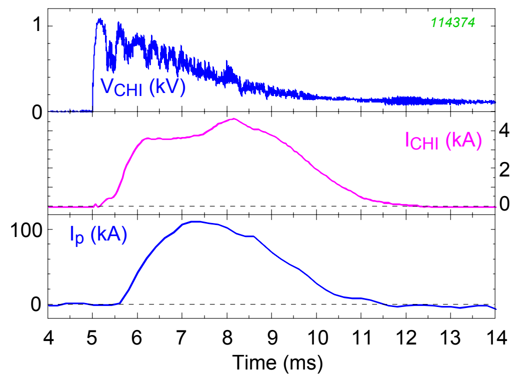

FIG.5 Time evolution of CHI plasma

kV was applied across the electrodes, generating an injector current of 4 kA and a resulting plasma current of 100 kA in this case. Plasma currents up to 140 kA with amplification factors (I_p/I_{CHI}) of up to 40 were achieved. This amplification factor is a factor of two greater than that obtained previously with longer duration CHI application. For the discharge shown in Fig. 5, T_i and T_e of 20 to 25 eV were measured. Flux closure is presently being assessed. Future work will focus on maintaining plasma current beyond the duration of the injector current.

3.2. Multi-Scale Transport

H-mode operation in NSTX resulted in the highest performance plasmas, with stored energies reaching 400 kJ in 1 MA plasmas with ~7 MW of NB heating power. An experiment to study the L-H threshold power was conducted as part of an NSTX/MAST identity experiment. The threshold power in NSTX was found to be low, P_{NBI} ~ 350 kW, in balanced DND plasmas at 0.5 MA and 0.45 T, with the threshold increasing to between 1 and 2 MW in LSN plasmas (∇B drift towards the X-point), consistent with MAST results for similar configurations and parameters [17]. Ohmic H-modes were often observed, and these exhibited a gradual decrease in the edge rotational shear and E_r starting up to 30 ms before the drop in D_α that signified the L-H transition.

The confinement trends in NSTX were similar to those at conventional aspect ratio in some respects, but differed in others. Systematic scans of LSN H-mode plasmas at fixed power and B_T indicated a linear increase in both the global and thermal τ_E, computed by EFIT and TRANSP respectively, as a function of plasma current (0.6 to 1.2 MA). At a fixed current of 0.8 MA, and 0.45 T, the global and thermal τ_E were found to scale as $P^{-0.40,\ -0.56}$ respectively, a slightly weaker degradation than at higher R/a. However, contrary to conventional aspect ratio, a strong B_T dependence was observed. This trend in the global and thermal confinement times is shown in Fig. 6. The left panel shows the global τ_E normalized to the 97 L-mode scaling [18], and the right panel shows the thermal τ_E normalized to the H-mode ITER98pby,2 thermal τ_E scaling [19]. The figures show that the global τ_E values are enhanced over the L-mode value, with enhancement factors of close to 2.8 at the highest B_T for both L- and H-mode and H-mode plasmas.

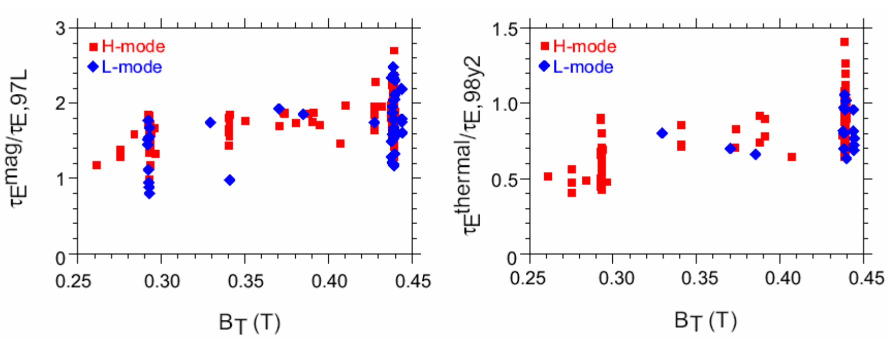

FIG. 6 Confinement enhancement factors relative to conventional R/a values for global and thermal τ_E for both L- and H-modes

The thermal confinement enhancement factors are more modest, reaching 1.4 at the highest B_T for H-mode plasmas, but plasmas, but with lower values at lower fields. Calculation uncertainties in the thermal τ_E are approximately 20%. The quality of the kinetic data at the lowest B_T precluded calculating the thermal τ_E at these fields with confidence. A reduction in confinement enhancement at the lowest B_T (<0.3 T) is seen for both the global and thermal values, and this reduction may be related to low-n MHD activity that is more prevalent at lower than at higher q. It is also seen that there is much scatter in the confinement enhancements at all fields.

Insight into the possible B_T dependence and processes causing transport can be gained by examining turbulence properties as measured by fixed frequency quadrature (30, 42 and 49 GHz) and swept (20 to 40 GHz) frequency correlation reflectometry systems, which, for the first time in NSTX and in an ST, was able to make quantitative long-λ turbulence measurements in the plasma core (r/a=0.2 to 0.7). Reflectometer phase fluctuations, which can be related to density fluctuations, were seen to correlate with global magnetic fluctuations over over a wide range of frequencies, as seen in Fig. 7. The phase and magnetic fluctuations (top panel) exhibit spectral peaks and moderate to high coherence (bottom panel) at similar frequencies. Turbulence radial correlation lengths have been measured deep in the plasma core where long-λ electrostatic modes are expected to be stable or suppressed by ExB fluctuations, and they are seen to be large, up to 20 cm, apparently resulting from the contribution by the magnetic fluctuations. Correlation lengths in the outer plasma (r/a=0.65) are smaller than in the core. In addition, the correlation lengths increased with decreasing B_T at fixed q, and the estimated density fluctuation levels (for frequencies >10 kHz and ignoring "obvious" coherent modes) also increased, with $\Delta n_e/n_e$~1.5% in the core for B_T=4.4 kG and ~4.3% for 3.25 kG. These general observations are consistent with reduced confinement at lower B_T. In the context of long-λ turbulence, then, finite β_T NSTX plasmas may represent a transition from an electrostatically dominated core to one where both localized and global magnetic fluctuations play a significant, if not dominant, role.

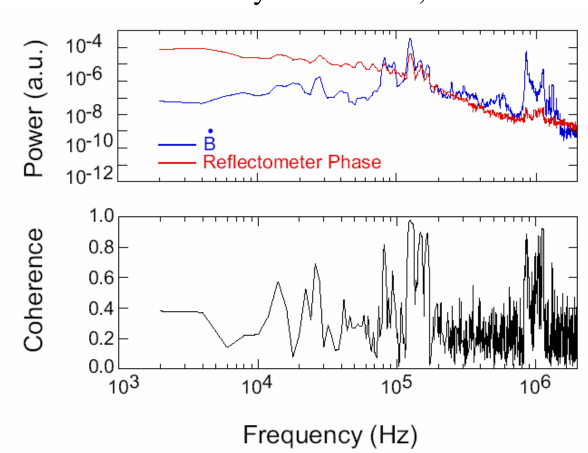

FIG. 7 Freqency spectra of magnetic and reflectometer phase fluctuations (top) Coherence between signals (bottom)

The determination of the transport properties of NSTX plasmas by TRANSP has benefited greatly by the increased number of spatial points of the CHERS diagnostic. The calculations indicate, as before [20], that the electron channel dominates the transport loss in most H-modes (χ_e = 10 to 20 m^2/s), with the ion thermal diffusivity near the NCLASS neoclassical value in many cases (χ_i = 1 to 5 m^2/s). NCLASS neoclassical values do not take into account enhancements to the neoclassical diffusivity by up to a factor of 2 due to finite orbit effects [21]. In the L-mode $\chi_i \approx \chi_e$ (~1 to 10 m^2/s) for line-averaged densities $\leq 4\cdot 10^{19}$ m^{-3}.

The local transport properties of NSTX plasmas appear to be sensitive to variations in magnetic shear, as is shown by comparing two discharges with different q-profiles. The q-profiles of these discharges were varied by changing the current ramp rate and the NBI timing in low density (n_{e0}~$2\cdot 10^{19}$ m^{-3}) L-mode discharges. In a discharge with a fast I_p ramp and early NBI, the T_i and T_e exhibited much stronger gradients near r/a=0.5 than in a discharge with a

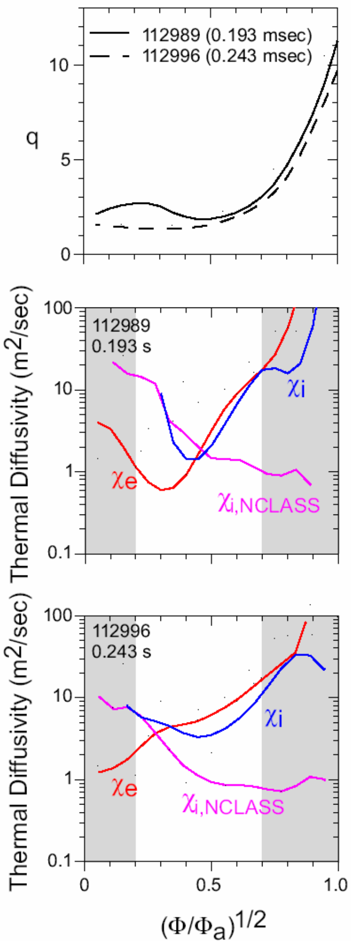

FIG. 8 Comparison of q profiles and thermal diffusivities for two low density L-mode discharges.

with a slower I_p ramp and later NBI, signifying an internal transport barrier. The q-profiles for these two discharges, as determined in TRANSP assuming Sauter neoclassical resistivity [22], is shown in the top panel of Fig. 8. The modeling for the slow ramp/late NBI discharge (112996) shows a monotonic q-profile, while that for the fast ramp/early NBI discharge (112989) exhibits a magnetic shear reversal from r/a=0.2 to 0.5. MSE measurements of the current profile to confirm the reversed shear were not available for these discharges. It is noted, however, that off axis 1/1 modes were observed in 112989, and similar modes were observed in discharges in which equilibrium reconstructions that used MSE measurement as a constraint did indicate reversed shear. The implications of the possible reversed shear are seen in the bottom panels of Fig. 8, which show a reduction by a factor of 3 to 7 in the thermal diffusivities of both the ions and electrons in the region of reversed shear. $\chi_i \approx \chi_e$ outside this region. Because of uncertainties in T_e, T_i and their gradients, the χs are highly uncertain in the shaded region, r/a<0.2 and >0.7.

Reflectometer measurements indicated both longer turbulence correlation lengths and higher estimated density fluctuation levels in the discharge with monotonic shear as compared to the one with possible reversed shear. In addition, gyrokinetic calculations indicate linear growth rates for ITG-TEM-ETG modes ($k_\theta \rho_s$=0.1 to 80) near r/a=0.45 which are significantly higher in the monotonic shear case and which exceed rotational rotational shear rates, with suppression of high $k_\theta \rho_s$ modes (ETGs) in the region of reversed shear [23]. Non-linear calculations are underway.

3.2. Waves and Energetic Particles

The 30 MHz (9^{th} $f_{c,D}^{+}$ harmonic on axis) system provides the potential for heating electrons selectively to reduce ohmic flux consumption and for providing non-inductive current drive directly. The twelve-strap HHFW antenna has the capability to launch waves over a range of wavenumbers ($k_{\|}$=3 to 14 m^{-1}) and directions. While significant electron heating has been observed in low density deuterium and helium plasmas, the actual power absorption of the electrons was found to depend sensitively on the spectrum of launched waves. Fig. 9 shows the results from a systematic power absorption study of the plasma response to modulated HHFW pulses of different phases. Both the % power absorption and incremental incremental confinement time in these HHFW-only plasmas were determined from the temporal response of the total stored energy to these modulations. The figure

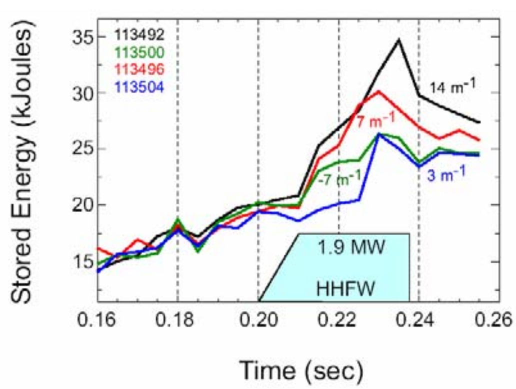

FIG. 9 Stored energy response to HHFW power modulation

figure shows a larger increase in the stored energy at shorter wavelengths ($k_{||}$=14 m^{-1}) with little initial response at $k_{||}$=3 m^{-1}. At 7 m^{-1}, a clear difference between co (-) and counter (+) current launch is seen. The % power absorption for determined from the responses is 80% at $k_{||}$=14 m^{-1}, 75%, 40% at 7, -7 m^{-1} respectively (counter, co-current injection) and ~10% at 3 m^{-1}, with the remainder of the power unaccounted for. Electron heating profiles are consistent with model calculations which predict broader heating profiles for higher $k_{||}$, but the increment in electron stored energy is less than what would be expected for pure electron heating.

Heating of the edge thermal ions was measured by the Edge Rotation Diagnostic [24], and this heating has been considered as a possible explanation for the apparent deficit in electron heating. This edge measurement indicates that the edge ions could be described as a two-temperature component plasma, with a significant hot component whose temperatures could reach 0.6 keV during HHFW heating. The edge ion heating was associated with parametric decay of the launched HHFW wave as measured by an RF probe. A frequency spectrum of the probe signal is shown in Fig. 10; the fundamental wave at 30 MHz is seen along with sidebands separated by $f_{c,D}$, indicative of a decay into an Ion Bernstein Wave (IBW) wave. More IBW sidebands are observed with increasing P_{HHFW}. While the edge ion heating is seen in conjunction with the IBW, only about 15% of the HHFW power went into the edge ions at P_{HHFW}=2 MW, independent of wave phasing. Consequently, the ion heating alone cannot explain the scaling of the power absorption. It is also noted that a significant amount of HHFW power could be absorbed by fast ions in HHFW+NBI experiments.

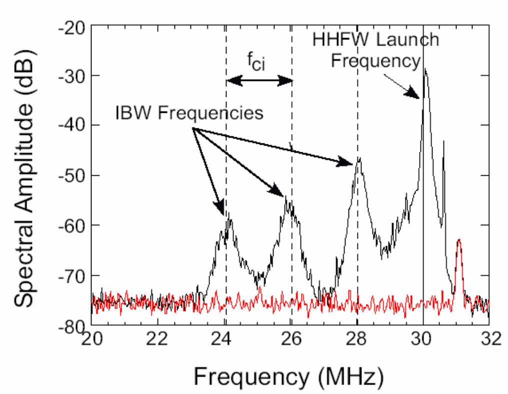

FIG. 10 Spectral power vs frequency showing parametric decay of the HHFW

The reduced HHFW power absorption limited the current driven by the HHFW, especially at $k_{||}$=3 m^{-1} where the driven current is predicted by theory to be maximal. Because of the importance of non-inductive current drive in STs, other techniques to accomplish this must be developed. The Electron Bernstein Wave (EBW) is one candidate. In this approach, an O-mode wave is converted to an EBW, which then heats the electrons locally at the cyclotron layer in the perpendicular direction. Modeling for high-β_T NSTX equilibria indicates that off-axis co-current is driven efficiently via the Ohkawa mechanism, in which passing electrons driving counter current become trapped [25,26]. The key to making this a viable technique is to have a >80% conversion efficiency from O-mode to the EBW. Assessments of EBW emission and estimates of mode conversion efficiency in NSTX support this requirement, and plans for developing a 3 MW EBW system are underway.

NSTX, and STs in general, are particularly susceptible to fast ion driven instabilities due to the intrinsically low B_T. The super-Alfvénic 80 kV neutral beam ions have similar dimensionless parameters to 3.5 MeV alpha particles from D–T fusion reactions in proposed magnetic fusion reactors. In NSTX, neutral beam heated plasmas typically exhibited a broad spectrum of instabilities excited through a resonant interaction with fast ions, from compressional and global Alfvén waves (CAE and GAE) at frequencies $0.3 < \omega/\omega_{ci} < 1$, to toroidal Alfvén eigenmodes (TAE) at frequencies ≈100 kHz. While there was no observed degradation in performance correlated with the appearance of CAE activity, enhanced fast ion losses were correlated with both the TAE-like and fishbone-like modes; this could be relevant to ITER in to ITER in the super-Alfvénic regime [27].

3.3. Plasma-Boundary Interface

The exploration of improved particle control and plasma fueling benefited from the implementation of several new techniques and capabilities. Boronization during 350C bakeout, occasional deposition of 1 to 2 g of boron prior to a run day and interspersing plasma and helium conditioning discharges helped to maintain good wall conditions and led to better density control. Initial experiments were successfully performed using a Li pellet injector developed for particle control and a supersonic gas injector for localized and efficient fueling. The use of these techniques will be expanded in future operation.

Because of the compact nature of the ST, it is important to not only account for the power escaping from the plasma but to reduce the power to the material surfaces. Power accountability in both LSN and DND plasmas was found to be good [28], with up to 80% and 90% of the power be accounted for in the two configurations respectively. The bulk of the power loss (35%) was deposited on the divertor plates, mostly in the outer divertor by up to a 5:1 ratio. Inner divertor detachment was found to reduce the power loading of the inner divertor plates to values of <1MW/m^2 [29]. Inner divertor detachment was observed in both L- and H-mode NBI-heated plasmas at densities >2·10^{19} m^{-3}. Fig. 11 shows an example of the inner divertor detachment; a cold, dense highly recombining and highly radiating MARFE-like plasma region developed on the inner divertor plate at 0.12 s, as indicated by a sharp increase in the D_γ/D_α ratio, an increase of the inner divertor radiation (bottom panel) and the appearance (not shown) of Stark-broadened Balmer series lines originating from n=5 to 10. The outer divertor in all experiments remained attached, with heat fluxes up to 10 MW/m^2 [30].

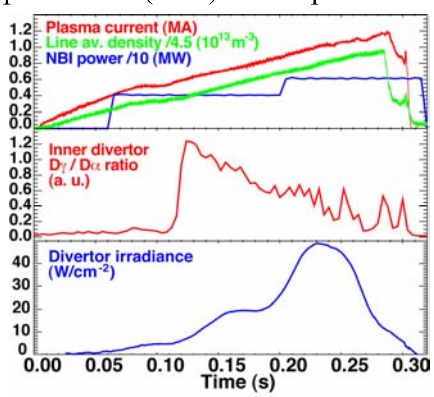

FIG. 11 Time evolution of a plasma discharge showing inner divertor detachment.

A variety of ELMS, which can cause increased divertor power loading, was observed in H-mode plasmas. A new type of ELM, Type V, was identified [31, 32]. This ELM is small amplitude with minimal energy loss, but could couple to Type I ELMS. The Type V ELM originates in the lower part of the vessel and propagates poloidally in the electron diamagnetic direction. The severity of ELMs that affect the plasma stored energy was found to depend sensitively on plasma elongation. Type I ELMs often exhibited low-n external kink-like structures. Future work will focus on understanding the underlying ELM stability properties and its dependence on shape using high spatial resolution edge diagnostics.

The 2-D structure of edge plasma turbulence was measured by viewing the emission of D_α or helium spectral lines enhanced by gas puffing using an ultra-high speed CCD camera [33]. Transitions from L-mode to H-mode could appear as a continuous evolution from a turbulent "blob-like" or intermittent state to a quiescent state over ≤ 0.1 ms, apparently without any new spatial features or flows. Transitions from H-mode to L-mode appeared as high-n poloidal perturbations which evolved into radially moving blobs. ELMs normally were associated with an increase in blob-like activity, although sometimes ELM-free H-modes had intermittent blob-like turbulence.

4. Integrated High Performance Scenarios

NSTX has made significant progress towards its goal of establishing the physics database at high β_T, with enhanced confinement and low ion transport levels, and mitigation of divertor heat loads. It has begun to develop an integrated understanding of how rotational and magnetic shear, as well as electromagnetic turbulence, affect performance. Despite outstanding issues in outstanding issues in understanding HHFW power deposition and fast ion confinement, other means to both generate and sustain current non-inductively have been explored. The advances over the past year in operational techniques to create favorable plasma profiles have led to significant progress towards the NSTX target of a high performance, non-inductively driven plasma. Fig. 12 reflects this progress statistically, where a crude estimate of bootstrap current fraction ($\varepsilon^{1/2}\beta_{pol}/2$) is plotted against β_T for NSTX discharges from the past four years of operation. The The target of high non-inductive fraction and high β_T is shown in the upper right hand corner. The red points were data taken during 2004, and as can be seen, a large step in both directions (shaded region) has been taken towards the target, with a significant number of discharges with both β_T>20% and with >40% estimated bootstrap fraction.

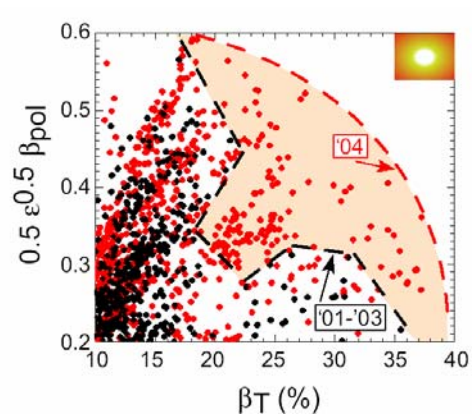

FIG. 12 Estimated bootstrap fraction vs β_T

A specific example of such an integrated high performance discharge is shown in Fig. 13. The greater shaping capability and early L-H transition in this discharge led to lower l_i and reduced ohmic flux consumption. This 1 MA discharge was heated by over 7 MW of NBI, and had a current flattop time of 0.8 s, which is approximately four current relaxation times. The stored energy of the plasma plateaued at 280 to 300 kJ and β_T at >20% for approximately 0.5 s, which is over ten τ_E. β_N exceeded 5 and τ_E/τ_{E97L} was about 1.7 simultaneously for the same duration. The line averaged density exhibited only a modest increase after t=0.3 s, and was then held constant at 80% of the Greenwald limit by ELM activity. n_e/n_{GW} reached 0.9 to 1 in other discharges, and no confinement degradation was observed at these high normalized densities.

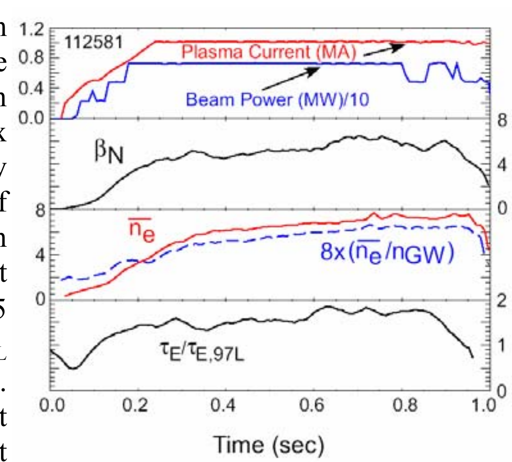

FIG. 13 Integrated high-performance discharge with significant non-inductive current

In this and similar discharges, the loop voltage remained low (<0.5 V) through the duration of the current and energy flattop, indicative of a significant amount of non-inductive driven current. Approximately 60% of the total current was driven non-inductively by beams (10%) and bootstrap (50%), as calculated by TRANSP. The MSE diagnostic, commissioned at the end of the 2004 run, will measure the current directly in order to aid in the assessment of the non-inductive current fraction and profile. Preliminary comparisons between the MSE measurements in the plasma core and profiles calculated by TRANSP show good agreement.

Acknowledgement

This research was supported by US DoE contract DE-AC02-76CH03073.

References

[1] ONO, M., et al., Nucl. Fusion **44** (2004) 452.
[2] PENG, M. et al., this conference.
[3] ONO, M., et al., Plasma Phys. Control. Fusion **45** (2003) A335.
[4] SYNAKOWSKI, E.J., et al., Nucl. Fusion **43** (2003) 1653.
[5] BELL, M. E., et al., Proc. 31st Eur. Physical Soc. Mtg on Plasma Physics (London 2004) Paper P2.194.
[6] LLOYD, B., et al., Nucl. Fusion **43** (2003) 1665.
[7] RAMAN, R., et al., Phys. Plasmas **11** (2004) 2565.
[8] GARTSKA, G.D., et al., Phys. Plasmas **10** (2003) 1705.
[9] MUELLER, D., et al., Proc. 31st Eur. Physical Soc. Mtg on Plasma Physics (London 2004) Paper P2.199.
[10] FERRON, J., et al., Nucl. Fusion **38** (1998) 1055.
[11] SABBAGH, S.A., et al., Nucl. Fusion **41** (2001) 1601.
[12] GATES, D.A., et al., Phys. Plasmas **10** (2003) 1659.
[13] WADE, M.R., et al., Nucl. Fusion **43** (2003) 634.
[14] MENARD, J., et al., this conference, Paper EX/P2-26.
[15] GLASSER, A.H and M.S. CHANCE, Bull. Am. Phys. Soc. **42** (1997) 1848.
[16] SABBAGH, S.A., et al., this conference, Paper EX/3-2.
[17] MEYER, H., et al., this conference, Paper EX/P3-8.
[18] KAYE, S.M., et al., Nucl. Fusion **37** (1997) 1303.
[19] THE ITER TEAM, Nucl. Fusion **39** (1999) 2137.
[20] LEBLANC, B.P., et al., Nucl. Fusion **44** (2004) 513.
[21] GATES, D.A. et al., Phys. Plasmas **11** (2004) L45.
[22] SAUTER, O., et al., Phys. Plasmas **6** (1999) 2834.
[23] STUTMAN, D., et al. this conference, Paper EX/P2-8.
[24] BIEWER, T., et al., Rev. Sci. Instrum. **75** (2004) 650.
[25] OHKAWA, T., General Atomics Report GA-A13847, unpublished (1976).
[26] TAYLOR, G., et al., Phys. Plasmas **11** (2004) 4733.
[27] FREDRICKSON, E., et al., this conference, Paper EX/5-3.
[28] PAUL, S.P., et al., J. Nucl. Mater., to be published, 2005.
[29] SOUKHANOVSKII, V., et al., J. Nucl. Mater., to be published, 2005.
[30] MAINGI, R., et al., Nucl. Fusion **43** (2003) 969.
[31] MAINGI, R., et al., J. Nucl. Mater., to be published, 2005.
[32] MAINGI, R. et al., this conference, Paper EX/2-2.
[33] ZWEBEN, S.J., et al., Nucl. Fusion **44** (2004) 1134.